Statistical Distribution of EVM Measurements for Direct-Modulation Radio-Over-Fiber Links Transporting OFDM Signals

Philippos Assimakopoulos, Anthony Nkansah, Nathan J. Gomes, *Senior Member, IEEE*, and David Wake, *Member, IEEE*

***Abstract*—The effect of distortion on the error vector magnitude (EVM) performance of orthogonal frequency-division multiplexing (OFDM) signals with different numbers of subcarriers and the connection to the peak-to-average power ratio (PAPR) of such signals is investigated. A low-cost and low-complexity directly modulated radio-over-fiber link is used in experiments as an example of a link limited by distortion. Statistical distributions of the EVM over a large number of transmitted OFDM frames are gained from experimental measurements and analyses of idealized processes. The measurement results show that as the number of subcarriers is reduced, the distribution means are more affected by extreme values. This effect results in mean EVMs for signals with different numbers of subcarriers that are not dependent in the expected way on the statistical PAPR of the transmitted OFDM signals. Instead, it is shown that in regions of moderate distortion, the median of the EVM is more closely related to the statistical PAPR and to the required back-off for signals with different numbers of subcarriers.**

***Index Terms*—Error vector magnitude (EVM), orthogonal frequency division multiplexing (OFDM), radio-over-fiber (RoF).**

I. Introduction

PREVIOUS WORK has shown that intensity modulated and directly detected (IM-DD) radio-over-fiber (RoF) links with external or direct modulation can offer good performance when transporting wireless signals employing orthogonal frequency division muliplexing (OFDM) modulation in the microwave and millimeter-wave frequency ranges. Examples of this approach include the transport of signals conforming to WiMAX and WiFi standards at microwave [1]–[4] and millimeter-wave [5], [6] frequencies, as well as those proposed for future mobile standards [7].

A metric that is often used in the literature for quantifying the performance of such links is the error vector magnitude (EVM) [1]–[6]. One of the limitations in the dynamic range of IM-DD architectures comes from distortion arising from nonlinear components in the transport architecture.

Manuscript received July 12, 2012; revised December 23, 2012; accepted January 02, 2013. This work was supported in part by the European Union project "FUTON" (FP7-ICT-2007-215533).

The authors are with the Broadband and Wireless Communications Group, University of Kent, Canterbury CT2 7NT, U.K. (e-mail: pa80@kent.ac.uk).

Color versions of one or more of the figures in this paper are available online at http://ieeexplore.ieee.org.

Digital Object Identifier 10.1109/TMTT.2013.2247615

In the case of directly modulated IM-DD links with transmission at microwave frequencies and short-to-medium reach, the major source of nonlinearity is the laser diode [8].

The transmission of OFDM signals through nonlinearities has been investigated extensively in the literature by using clipping and other simple nonlinear models [9]–[14].

Specifically for RoF implementations, the effects of the nonlinearity of a Mach–Zehnder external modulator [15], [16] and that of a directly modulated laser diode using a simple polynomial model and making use of the output autocorrelation function [17] have been investigated, while in [18], a comparison between a clipping function and such an RoF link with a laser diode at low bias was carried out.

However, very little work [14], [19] has been carried out on exploring the effects of different numbers of subcarriers, and whether this results in a variation of required input power back-off due to changes in the peak-to-average power ratio (PAPR). In [19], a difference in back-off from the 1-dB compression point of 0.5 dB at 4% EVM between 64–2048 OFDM subcarriers was reported for a directly modulated RoF link. However, this comparison was not optimized for exploring the effects of different numbers of subcarriers. Different signal generation and equalization techniques were used and the comparison was carried out over a relatively small number of transmitted OFDM frames.

In this paper, the goal is to investigate whether differences in the PAPR between signals with different numbers of subcarriers lead to differences in the input power back-off required to maintain EVM performance. Section II covers the basic theory of OFDM and presents the predictions of the statistical PAPR for different numbers of OFDM subcarriers. Statistical analyses of the measured EVM results are then carried out from two perspectives: the first examines the distribution of the mean EVM in each transmitted OFDM frame; the second examines the distribution of the EVM of every subcarrier in all of the transmitted frames. The methodology is described in Section III. Section IV describes the RoF link-based measurement setup and presents EVM measurement results. Sections V and VI then present the results of the statistical analyses on the measured EVM for the two distributions of interest.

Note that while the mean of the EVM can in principle be estimated analytically (from the signal-to-noise ratio) using statistical models [12], [15], [17], [18], [20], the aim here is to obtain the EVM distributions directly from measurements and

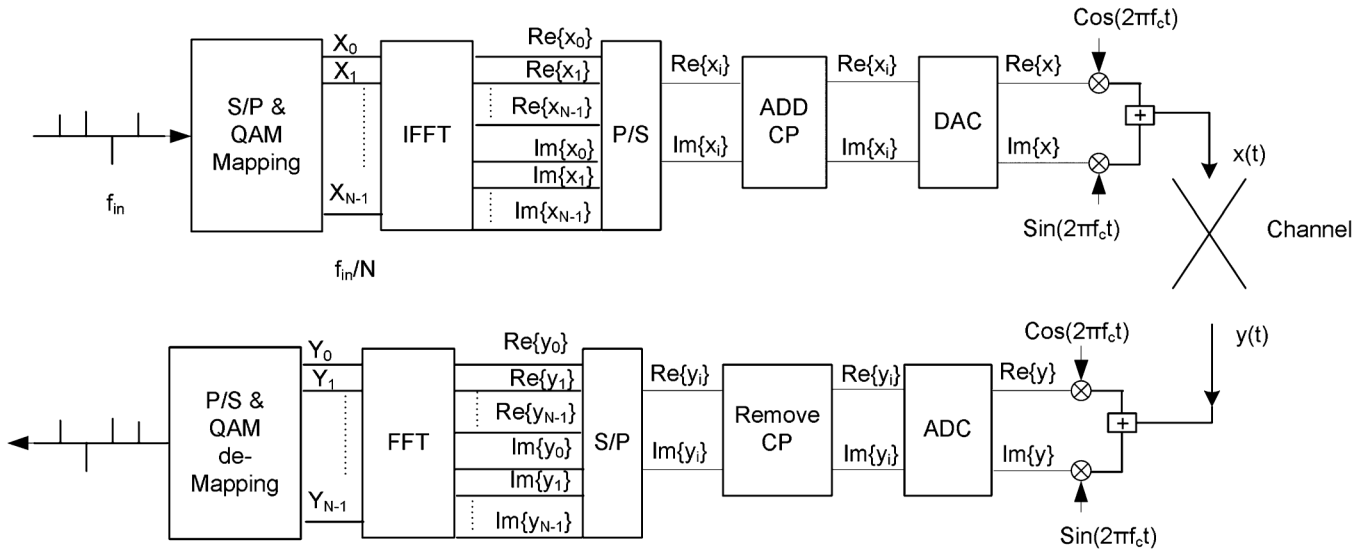

Fig. 1. OFDM transmitter and receiver architectures.

avoid any inherent approximations resulting from such a modeling process.

II. OFDM AND PAPR THEORY

The objective of this section is to examine the variation of PAPR with the number of OFDM subcarriers. Once this is done, the PAPR results can be related to the EVM performance to be presented in the following sections.

A simplified block diagram for the transmitter and receiver sections of an OFDM system is shown in Fig. 1. Upper case characters are used for frequency-domain samples, while lower case characters are used for time-domain samples. The input data bits arrive at a certain rate (f_{in}), go through a serial-to-parallel (S/P) conversion, and are mapped to quadrature amplitude modulation (QAM) constellation points. The resulting QAM symbols form the vector of frequency-domain samples $[X_0\, X_1 \ldots X_{N-1}]^T$. At this point, the rate of the samples is reduced by the inverse fast Fourier transform (IFFT) size. The frequency-domain samples then go through the IFFT block, which produces the vector of time-domain samples $[x_0\, x_1 \ldots x_{N-1}]^T$. After parallel-to-serial (P/S) conversion, a cyclic prefix (CP) is appended at the beginning of each OFDM symbol. The resulting frames (note that the term "frame" is used here to denote an OFDM symbol that has a CP appended to it) then go through a digital-to-analog converter (DAC) before being up-converted to passband (modulating the RF carrier) for transmission through a physical channel. At the receiver, the opposite processes are carried out to retrieve the original QAM symbols.

The output of the IFFT modulator is given by [22]

$$x[n] = \frac{1}{\sqrt{N}} \sum_{k=0}^{N-1} \left[|X[k]| \cos\left(\frac{2\pi kn}{N}\right) + \arg(X[k]) \right] + j\frac{1}{\sqrt{N}} \sum_{k=0}^{N-1} \left[|X[k]| \sin\left(\frac{2\pi kn}{N}\right) + \arg(X[k]) \right] \quad (1)$$

where $x[n]$ are the time-domain samples and $X[k]$ are the frequency-domain samples at the output and input of the IFFT block, respectively.

The absolute PAPR over one OFDM frame before the DAC is given by [23]

$$\text{PAPR}(x[n])_{0-N-1} = \frac{\max |x[n]|^2}{E\{|x[n]|^2\}} \leq N \frac{\max |X[k]|^2}{E\{|X[k]|^2\}} \quad (2)$$

where $E\{\cdot\}$ is the expectation operator.

In the case of quadrature phase-shift keying (QPSK) modulation, the equality in (2) is obtained when $X[k]$ have the same phase. The term absolute is used here to differentiate this quantity from the statistical PAPR that will be presented shortly. From (2), the absolute PAPR with QPSK modulation will have a value of N. For example, for a 256-subcarrier system, the absolute PAPR will be equal to 24.1 dB. However, all the carriers being in phase is a highly improbable condition, and therefore it is usually neglected. System designers usually assume PAPR values that are more practical and stem from a statistical analysis of the signal waveform. Assuming the underlying processes acting on the in-phase and quadrature components of (1) are independent and identically distributed (i.i.d.), the $X[k]$ will also be i.i.d. As the number of subcarriers increases, the central limit theorem (CLT) ([21, p. 214]) can be invoked: in-phase and quadrature components tend to zero mean Gaussian variables with variance σ^2. The envelope, $|x[n]| = r$, corresponding to the magnitude of the uncorrelated in-phase and quadrature components becomes Rayleigh distributed with parameter σ. The complementary cumulative distribution function (CCDF) of the PAPR over n samples at the output of the IFFT modulator will be given by [23]

$$P(\text{PAPR} > z) = 1 - (1 - e^{-z})^n \quad (3)$$

where $z = r^2/2\sigma^2$. For $n = N$, (3) gives the statistical PAPR per OFDM frame.

When the OFDM signal goes through the DAC (assuming it has sufficient dynamic range and does not itself limit the peaks),

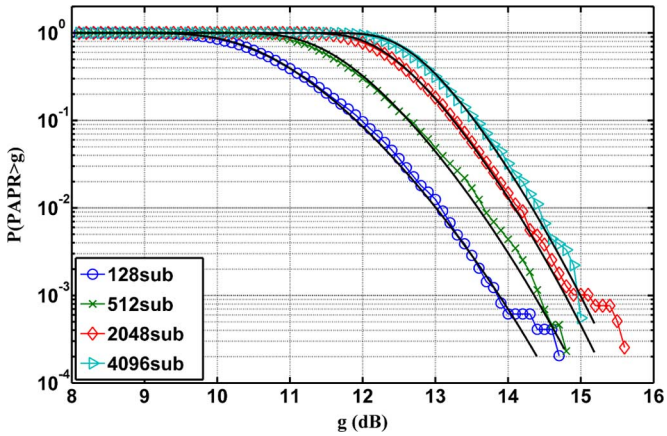

Fig. 2. CCDF plots of the PAPR of the up-converted OFDM signal. Solid lines are the theoretical results from (5), point traces are simulation results.

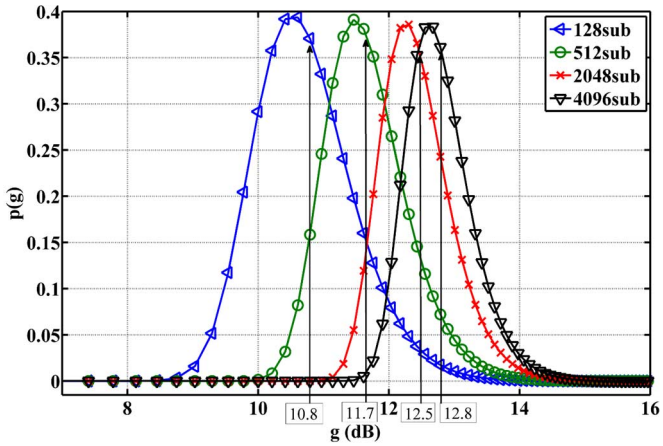

Fig. 3. PDF of PAPR of 128, 512, 2048, and 4096 subcarriers. The medians of each distribution are indicated.

some peak regrowth may occur [23]. This can be avoided with the use of oversampling. In that case, (3) will underestimate the PAPR, and for this reason, a factor, determined by simulations, is used in [24] to increase n.

Equation (3) describes the statistics of the PAPR of the baseband OFDM signal, but in RoF systems it is the up-converted signal (modulating an RF carrier) that modulates the laser diode. The up-converted signal can be described as a narrowband random process of the form [25]

$$x(t) = r(t) \times \cos[2\pi f_c t + \Phi(t)] \tag{4}$$

where $\Phi(t)$ is the phase with a uniform distribution $\sim[0 - 2\pi]$ and f_c is the RF carrier frequency. As (4) comprises the multiplication of two random variables, the envelope, $r(t)$, with a Rayleigh distribution, and the random phase, $\Phi(t)$, with a cosine distribution, the resulting distribution is Gaussian. Thus, the CCDF of the PAPR per OFDM frame can be given directly in terms of the Gaussian distribution of the up-converted signal

$$P(\text{PAPR} > g) = 1 - \left\{\frac{1}{2} \times \left[1 + \text{erf}\left(\sqrt{\frac{g}{2}}\right)\right]\right\}^{lN} \tag{5}$$

where erf is the error function, $g = x^2(t)/\sigma^2$, and l is a factor empirically estimated (through simulations).

Fig. 2 shows the statistical PAPR given by (5) for 128 subcarriers ($l = 23$), 512 subcarriers ($l = 27$), 2048 subcarriers ($l = 29$), and 4096 subcarriers ($l = 31$). Also shown, for comparison, is the PAPR obtained from a simulation in MATLAB, carried out by generating, oversampling by a factor of 4, and up-converting 4000 frames for each IFFT size, and by then calculating the PAPR for each frame. The factor, l, and the one in [24] are related. The main difference between them is that, in [24], it is used to fit the baseband PAPR, while in this paper, it is used for the passband PAPR. Also, in [24], the authors provide a single value for this correction factor for all IFFT sizes (a single value that provides the closest match between theoretical and simulation results for all IFFT sizes), while in this paper, a different value is given for this factor for each IFFT size.

The probability distribution function (PDF) of the PAPR is given by

$$p_{\text{PAPR}}(g) = \frac{d}{dg}\left\{\left[\frac{1}{2} \times \left[1 + \text{erf}\left(\sqrt{\frac{g}{2}}\right)\right]\right]^{lN}\right\}. \tag{6}$$

The result of (6) is shown in Fig. 3 for the CCDFs of Fig. 2. Also shown in Fig. 3 are the median points of the distributions. For IFFT sizes up to 2048, the median increases by approximately 0.4 dB for each doubling of the number of subcarriers. Above 2048 subcarriers, this value reduces to approximately 0.3 dB.

These results show that while the instantaneous amplitude of the envelope of the multicarrier signal may be much higher than the envelope average, the instantaneous envelope variations are completely quantified through the statistical PAPR analysis. It is also evident from Fig. 2 that all the subcarriers being in phase and giving the highest theoretically possible instantaneous amplitude is an extremely improbable event.

III. Statistical Methodology

Transmission of the OFDM radio signals will lead to the addition of a noise contribution, $n'(t)$, and a distortion component, $d(t)$. In the case of the directly modulated RoF link presented in Section IV, the noise arises from laser diode relative intensity noise (RIN), photodiode (PD) thermal, and shot noise; the distortion is mainly caused by laser diode nonlinearity. Other distortion mechanisms that may depend on the optoelectronic component used (e.g., Fabry–Perot or vertical-cavity surface emitting laser diodes) such as fiber dispersion in conjunction with laser chirp, are not investigated in this paper, but it is assumed that, for short-to-medium reach applications, relatively small-signal bandwidths (<40 MHz) and frequencies of operation in the microwave range, dispersion will not make a large contribution to the system performance.

After an appropriate equalization technique has been used to equalize the link frequency response, the signal at the output of the receiver FFT will be given by

$$Y[k] = S[k] + (D[k] + N'[k]) = S[k] + N[k] \tag{7}$$

where

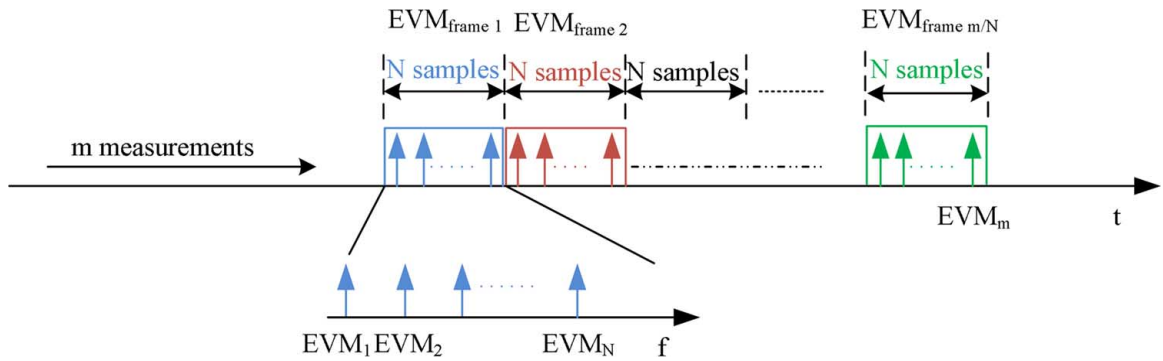

Fig. 4. Diagram showing how the EVM measurement results are interpreted for the employed statistical methodology.

$$S[k] = \frac{1}{\sqrt{N}} \times \sum_{n=0}^{N-1} s[n] \times e^{-\frac{j2\pi kn}{N}} \tag{8}$$

$$N[k] = \frac{1}{\sqrt{N}} \times \sum_{n=0}^{N-1} n[n] \times e^{-\frac{j2\pi kn}{N}}. \tag{9}$$

The first part on the right-hand side of (7) represents the useful signal sample, $S[k]$, while the terms in brackets represent the samples of the distortion, $D[k]$, and noise contributions, $N'[k]$, at the location of subcarrier k. Equation (7) assumes an additive noise process that is uncorrelated with the output signal. This assumption is only valid for an input whose amplitude follows a Gaussian distribution [9], [10]. It does not hold otherwise (e.g., for single-carrier QAM).

There are two statistical distributions of interest. The first is the distribution of the mean EVM of every transmitted OFDM frame (where each mean EVM value is obtained by averaging across the EVM values of all the subcarriers within the frame). This distribution is termed the *EVM per frame* distribution. The second is the distribution of all of the EVM values, i.e., of every OFDM subcarrier in every transmitted OFDM frame. This is termed the *raw EVM* distribution. Fig. 4 shows how the results from an EVM measurement are interpreted for the analysis that will follow. A long time series of m EVM measurements is obtained. Each of these measurements is a raw EVM value (EVM_1 to EVM_m). As the OFDM signal demodulation is inherently done per frame, there are sets of N contiguous values from this time series, which are from the same frame, where N is the number of data subcarriers in the measured OFDM frame. In this way, the measurements are partitioned into sample sizes equal to the number of data subcarriers in the received OFDM frame. Therefore, in addition to the raw EVM values, a set of m/N mean values are obtained, which represent the EVM per frame values. The raw EVM values within each frame correspond to different frequencies within the signal band and are "received" simultaneously (as they belong to the same frame), but due to the P/S conversion in the receiver section of Fig. 1, these measurements are separated in time. The EVM for subcarrier r is given by

$$\mathrm{EVM}_r = \sqrt{\frac{P_{N[r]}}{\bar{P}}} = \frac{\sqrt{[\mathrm{Re}\{N[r]\}]^2 + [\mathrm{Im}\{N[r]\}]^2}}{v_{\mathrm{rms}}} \xrightarrow{\text{tends}} \mathrm{Rayleigh}(\sigma'), \quad \text{for } r = 1, 2, \ldots, m \tag{10}$$

where $P_{N[r]}$ is the power of the total noise sample (i.e., including distortion and other noise contributions) in subcarrier r, $\bar{P}$ is the mean power of the constellation and σ' is the standard deviation of the in-phase and quadrature components of the total noise contribution.

Note that now the frequency index k is replaced with the index r, to reflect the change to a time-domain representation for the measurement results in accordance with the representation of Fig. 4. The real and imaginary components in the numerator of (10) will tend to Gaussian distributions due to the averaging in the receiver fast Fourier transform (FFT) and the CLT, as N is large. Therefore, the numerator being the magnitude of the two components will tend to a Rayleigh distribution. Since this is at the output of the FFT, the v_{rms} term is the root-mean-square voltage of the constellation.

The measured EVM per frame is the arithmetic mean over a whole frame

$$\mathrm{EVM}_f = \frac{1}{N} \times \sum_{r=(f-1)N+1}^{fN} \left(\sqrt{\frac{P_{N[r]}}{\bar{P}}} \right) \xrightarrow{\text{tends}} \mathcal{N}(\mu_f, \sigma_f), \quad \text{for } f = 1, 2, \ldots, \frac{m}{N} \tag{11}$$

where N is the number of data subcarriers in the frame.

Assuming that the raw EVM is an i.i.d. process, with mean μ_r and variance σ_r^2, the EVM per frame will have a mean μ_f and variance σ_f^2 given by

$$\mu_f = \mu_r \tag{12}$$

$$\sigma_f^2 = \frac{\sigma_r^2}{N}. \tag{13}$$

Equations (12) and (13) are a direct result of the Weak Law of Large Numbers [21]. They show that the EVM per frame will have a variance inversely dependent on the number of subcarriers, and a mean equal to the mean of the raw EVM distribution. In terms of estimation theory, it can be said that μ_f is an unbiased estimator of the mean of the raw EVM, while σ_f^2 is a biased estimator of the variance of the raw EVM. Additionally, as N is large, due to the CLT, the distribution of the EVM per frame will converge to a Gaussian distribution.

In the literature, it is often assumed that the effects of distortion (above some input power level) are equivalent to those of an i.i.d. white noise process [20], [26]. But, when distortion

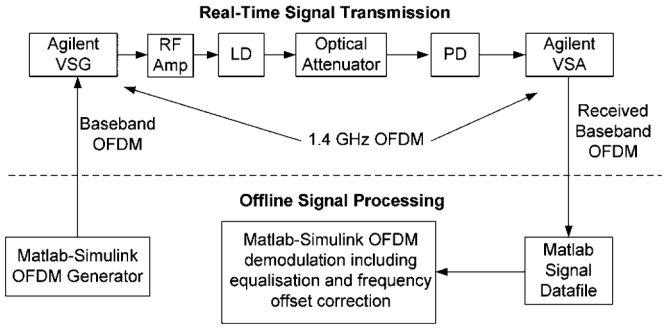

Fig. 5. Detailed flowchart of the measurement procedure. RF amplifier: RF Amp. Laser diode: LD. Photodiode: PD.

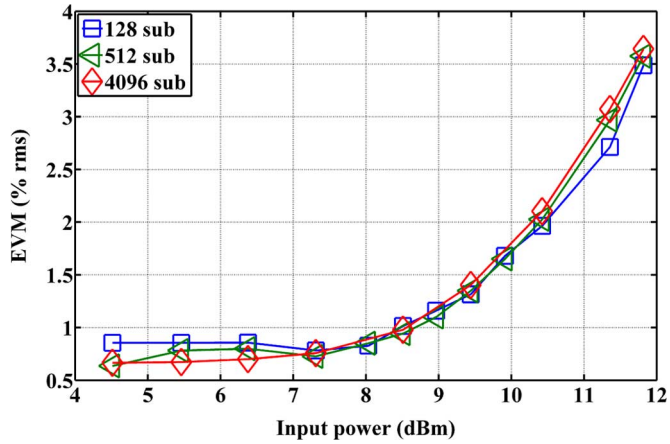

Fig. 6. EVM as a percentage (%) of the rms amplitude of the constellation versus input power for different numbers of subcarriers with QPSK modulation over 450 OFDM frames.

takes effect, this assumption may not hold. The aim of the following sections is to see whether (and under which conditions) the raw EVM distribution will converge to a Rayleigh distribution in accordance with (10) and whether the EVM per frame will conform to (12) and (13), and also converge to a Gaussian distribution.

IV. Experimental Measurements

The measurement setup and procedure are illustrated in Fig. 5. The baseband OFDM signal is generated in MATLAB-Simulink and is then downloaded to an Agilent vector signal generator (VSG), which performs RF up-conversion. The up-converted signal directly modulates a Teradian distributed feedback (DFB) laser and the resulting modulated light is transmitted through a 10-dB optical attenuator (emulating optical losses in fiber, connectors, etc.) and short length of fiber patch-cord before being directly received by an Appointech p-i-n PD. The optical attenuator also ensures that the PD is not saturated by the incident optical signal. An RF amplifier is used at the input of the optical link in order to control the input RF power into the laser diode. The signal is then received by an Agilent vector signal analyzer (VSA) where it is down-converted and saved as a MATLAB data file for offline signal processing. Note that the VSG and VSA internal attenuators were set such that their DAC and analog-to-digital converter, respectively, are not driven into saturation by the input OFDM signal. The offline processing includes timing synchronization, blind equalization, and blind frequency offset correction. The generated OFDM signals have a bandwidth of 20 MHz and the RF frequency is 1.4 GHz. The ratio of data carriers to zeros (null subcarriers) is based on the WiMAX specifications [27], except for the case of 128 subcarriers, where 16 zeros are used. A short CP is used at a ratio of 1/8 of the symbol duration. Any distortion observed will be mainly due to the laser diode, as both the VSG and RF amplifier were operated far below their individual compression points. The input 1-dB compression point (P1 dB) of the RoF link with no RF amplifiers was measured as 19 dBm.

The measured results in this section are obtained as follows: at every RF input power, 450 OFDM frames are transmitted, and for each frame, the mean EVM is calculated by averaging across the EVM values of all the subcarriers within the frame. The final EVM result for each RF input power is the average of all the mean EVMs transmitted at that particular RF input power. A form of averaging across the subcarriers of each frame is typically employed when calculating the EVM of any transmission system in the literature [28], and it is the way it is implemented in measurement equipment, such as VSAs.

Fig. 6 shows the measured EVM, given as a percentage (%) of the rms amplitude of the constellation, versus input power result for different numbers of subcarriers (128, 512, and 4096 subcarriers) with QPSK modulation, measured over 450 OFDM frames. Wireless standards usually define EVM transmitter requirements, and an appropriate input power can be chosen so that the EVM will meet a specified requirement. Generally then, the input power can be reduced in order to maintain an EVM below the specified limit, and the input power can therefore be expressed in terms of a power back-off from P1 dB of the optical link. It is seen in Fig. 6 that as the input RF power is increased to a level closer to P1 dB (19 dBm), distortion begins to dominate the performance and the EVM increases at a high rate. The back-off requirements are almost the same for the different numbers of subcarriers. In terms of the EVM turning point (the point where the EVM starts to rise quickly due to distortion), a back-off of 12 dB from the 19-dBm P1 dB is close to the expected value of the median of the statistical PAPR result (Fig. 3). However, the expected difference in the required back-off due to the variation of statistical PAPR with different numbers of subcarriers (Fig. 3) is not observed in this result.

In general, following the transmission through the optical link, signals will be transmitted through a wireless channel. Therefore, the optical link should have a minimum effect (in terms of performance degradation) on the quality of the transmitted signals. Thus, here, we are mostly interested in the relatively low EVM distortion limited range. Higher input powers will be investigated in terms of the statistics of the EVM results in the following sections.

Fig. 7 is a plot of the EVM variance with input power. Although the mean EVM is almost the same for different numbers of subcarriers, the variance is not. As expressed in (13), the EVM variance is higher for lower numbers of subcarriers.

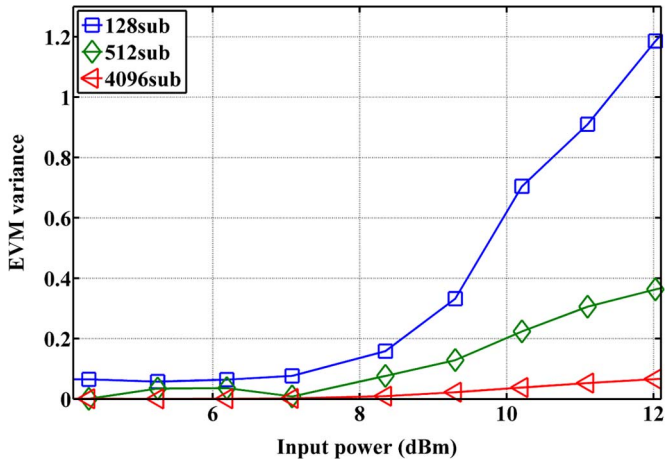

Fig. 7. EVM variance for different numbers of subcarriers.

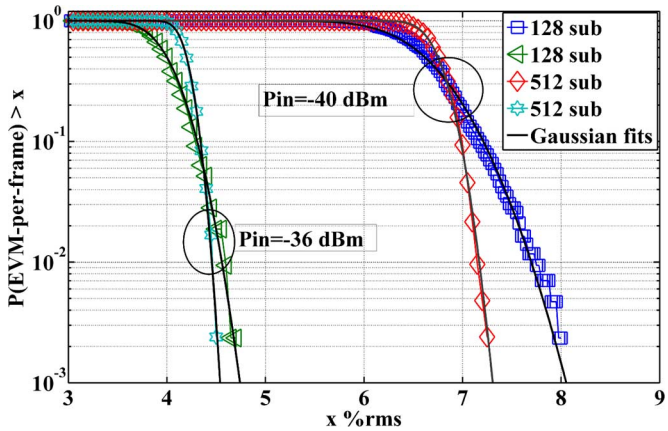

Fig. 8. EVM per frame CCDFs for 128 and 512 subcarriers at two input powers at the noise limited end of the EVM. The distributions have equal means, but the standard deviation of 128 subcarriers is approximately double that of 512 subcarriers.

TABLE I
SUMMARY OF FITTED NORMAL DISTRIBUTION PARAMETERS (MEAN AND STANDARD DEVIATION) FOR THE NOISE-LIMITED END PERFORMANCE (FIG. 8)

	-40 dBm		-36 dBm	
Subcarrier number	σ	m	σ	m
128	0.4	6.65	0.2	4.2
512	0.19	6.72	0.11	4.1

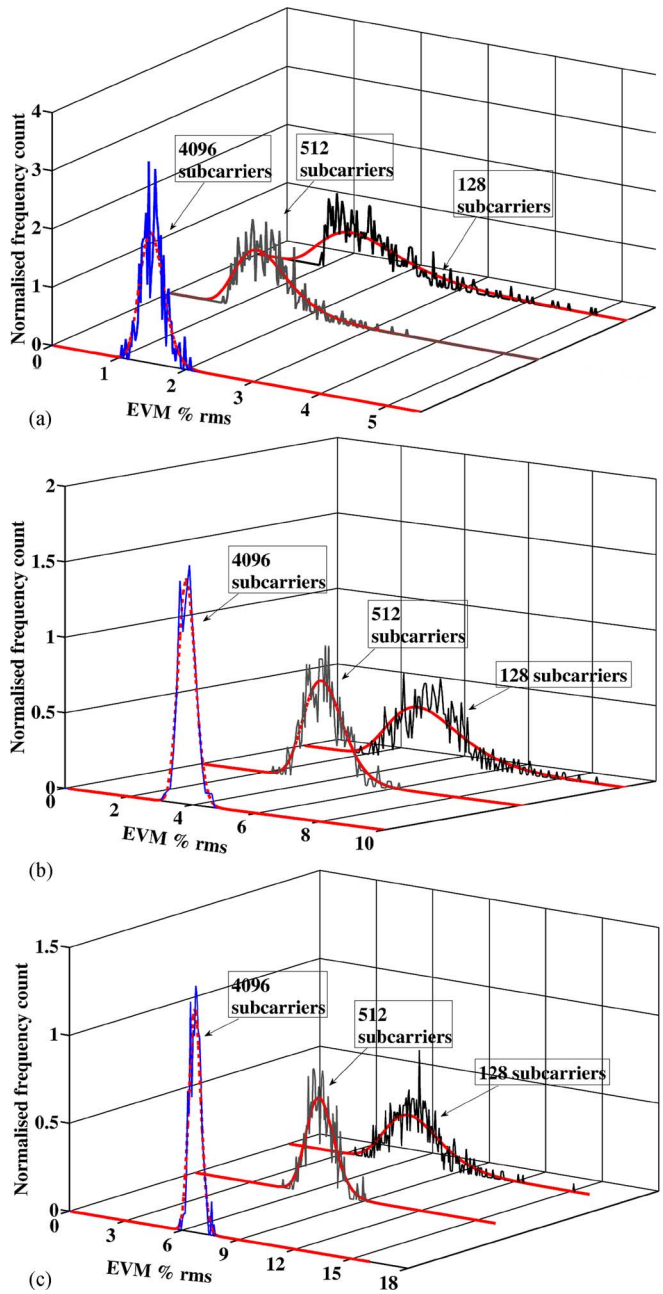

Fig. 9. Histogram plot of the average EVM per frame over 450 frames for 128, 512, and 4096 subcarriers at input powers of: (a) 9.45 dBm, (b) 11.8 dBm, and (c) 13.6 dBm with fitted log-normal distributions.

V. EVM PER FRAME DISTRIBUTIONS

In Fig. 8, plots of the CCDFs of the EVM per frame for 128 and 512 subcarriers, with Gaussian fits for operating points in the noise-limited region (i.e., negligible distortion) of the EVM measurements are presented. It can be seen that the distributions are approximately Gaussian. At each input power, the means are approximately equal, while, in agreement with (13), the standard deviations for the 128 subcarrier results are approximately double that of the 512 subcarriers results (see the fitting parameters presented in Table I).

Fig. 9 shows histogram plots of the EVM per frame for 128, 512, and 4096 subcarriers over 450 frames at input RF signal powers into the laser diode of 9.45, 11.8, and 13.6 dBm. These input powers are within 10 dB from the P1 dB of the link and thus all correspond to operation where distortion from the link dominates the performance. In general, it can be seen that the lower of these powers and the lower numbers of subcarriers lead to more positively skewed distributions (for a description of statistical skewness see [29. p. 47]. The measured distributions can be better approximated by log-normal distributions [30] that match the positive skew quite adequately. The fitted distributions (dashed traces) are shown superimposed on the histograms. Note that the fitting becomes worse as the input power is reduced (this is a result of nonideal equalization). The fitting with the log-normal distributions is carried out using the

TABLE II
SUMMARY OF FITTED LOG-NORMAL DISTRIBUTION PARAMETERS: σ^2 IS THE VARIANCE, μ IS THE MEDIAN, AND m IS THE MEAN

	9.45 dBm			11.8 dBm			13.6 dBm		
Sub no.	σ^2	m	μ	σ^2	m	μ	σ^2	m	μ
128	0.57	1.7	1.57	1.6	4.12	3.94	2.33	6.85	6.69
512	0.2	1.5	1.45	0.4	3.91	3.86	0.55	6.73	6.69
4096	0.03	1.5	1.49	0.07	3.83	3.82	0.1	6.7	6.69

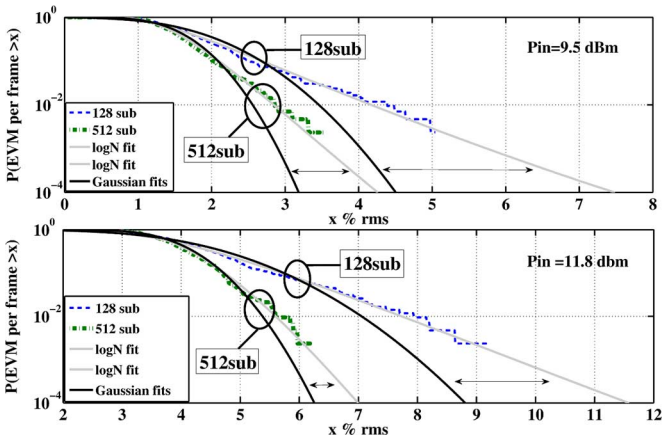

Fig. 10. Comparison of measured CCDFs with normal CCDFs.

CDFs of the measured distributions. Note also that for practical reasons (differences in the variance between the different IFFT sizes), these plots have different scales in their x-axis. This makes more clearly visible the important information obtained from these results, which is the difference in the skew between these distributions. From Fig. 9, it is seen that the left tail of the distribution is bounded, i.e., the EVM cannot be lower than some value, while the right tail is unbounded. Table II summarizes the fitted parameters (mean, median, and variance) for the log-normal distributions shown in Fig. 9.

Fig. 10 shows the differences in the tails of the distributions with those of normal distributions (for the same mean and variance). As the input power is increased, the heaviness of the tail reduces and the distributions tend to Gaussian distributions, as predicted by (11).

Fig. 11 shows this in terms of the reduction of the skew of the distributions for high powers and high numbers of subcarriers. It can also be noted that the skew peaks at some input power due to the onset of distortion before a trend of reduction is observed. Generally, it is these regions of large skew that are of most interest when analyzing the limitations to EVM performance due to distortion.

The fact that the distributions are skewed and not Gaussian is due to the grouping of subcarriers into frames (which is simply how OFDM modulation and demodulation operate). An OFDM frame with high PAPR will lead to a higher mean EVM for that specific frame as the distortion will generally affect the whole frame. This will lead to some frames with a high mean EVM, resulting in the extreme values observed in the distributions.

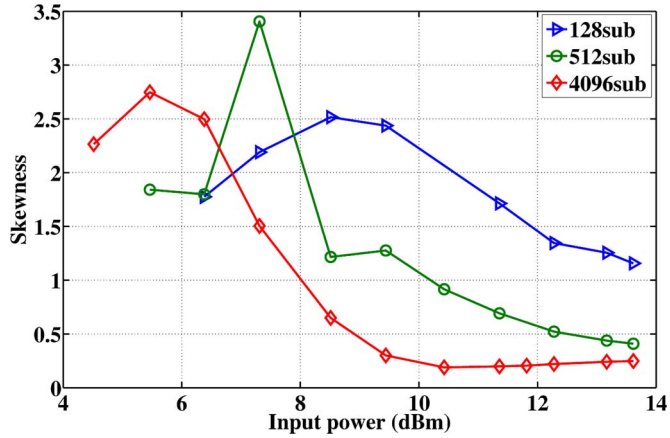

Fig. 11. Skew of the distributions at different input powers.

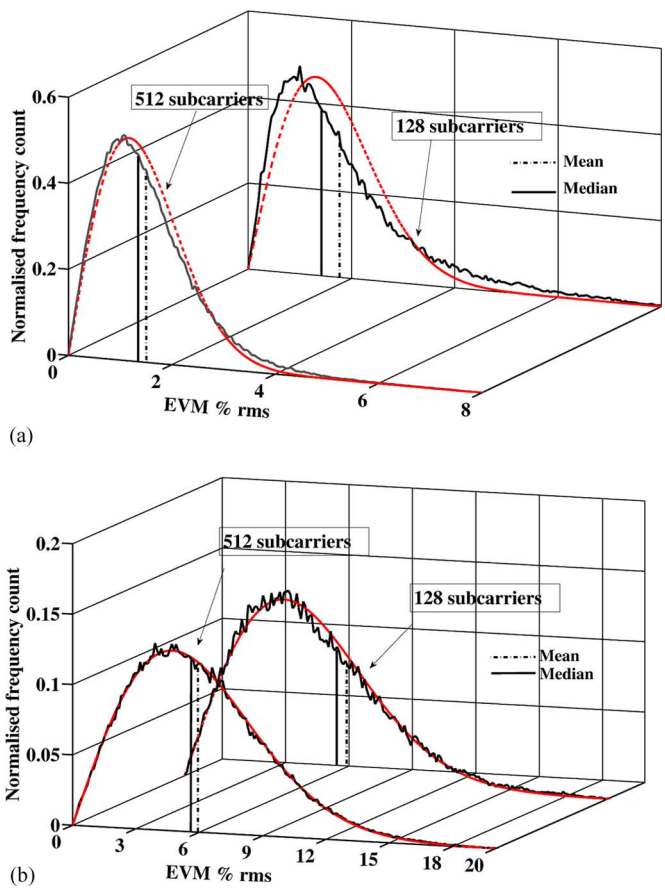

Fig. 12. Distributions of the raw EVM for 128 and 512 subcarriers at input powers of: (a) 9.45 dBm and (b) 13.2 dBm. The dashed traces are Rayleigh fits.

VI. RAW EVM DISTRIBUTIONS

Fig. 12 shows plots of the raw EVM distributions for 128 and 512 subcarriers with fitted Rayleigh distributions in accordance with (10), at input powers of 9.45 and 13.2 dBm. It can be seen that the fitting with the Rayleigh distributions becomes less accurate as the input power and/or number of subcarriers are reduced. This can be seen in Table III that summarizes goodness of fit parameters for the distributions. Both error parameters reduce with input power and number of subcarriers. This has to do with the characteristics of the distortion. At intermediate input

TABLE III
GOODNESS OF FIT MEASURES FOR THE FITTING BETWEEN THE RAW EVM DISTRIBUTIONS AND THE RAYLEIGH DISTRIBUTIONS. STANDARD SQUARED ERROR: SSE, ROOT MEAN SQUARE ERROR: RMSE

	9.45 dBm		11.35 dBm		13.2 dBm	
Sub no.	**128**	**512**	**128**	**512**	**128**	**512**
SSE	1.26	0.15	0.4	3.7e-2	9.9e-2	8.4e-3
RMSE	3.7e-2	1.5e-2	1.7e-2	6e-3	7e-3	2.2e-3

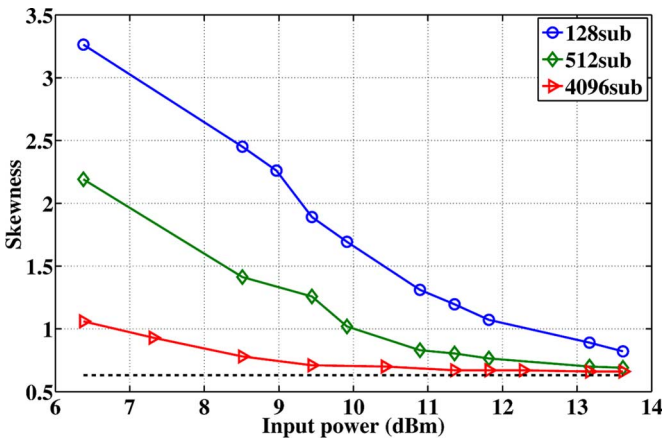

Fig. 13. Skew of the raw EVM distributions for 128, 512, and 4096 subcarriers. The dashed trace is the Rayleigh distribution skew.

powers, as distortion starts to affect the performance, the skew in the statistical distributions increases until it reaches a peak. Due to the increased skew, the distributions are not Rayleigh distributions and this effect is more pronounced as the IFFT size is reduced. As the input power is further increased, the skew reduces (to that expected by a Rayleigh distribution) and the measurement result is closer to that expected from theory. The skew in the Rayleigh distributions is an indication that the real and imaginary components in the numerator of (10) are not normally distributed, but with distortion have a positive skew. Note that the mechanism that causes the skew in these distributions is different from that in the case of the EVM per frame distributions of Section V.

Fig. 13 shows the skew of the raw EVM distributions. The dashed trace represents the Rayleigh distribution limit for this statistical measure. Higher skew results in an increase in the distance between the mean and the median. For example, assuming that the variance of the real and imaginary components in the numerator of (10) is lower for signals with a lower number of subcarriers (as would be expected due to the lower statistical PAPR result), the higher skew for these signals will result in a greater difference between mean and median compared to signals with more subcarriers (as can be observed in Fig. 12). Thus, as these distributions possess different amounts of skew, the mean is not the best measure of performance and instead the median should be used.

Fig. 14 shows the result for both the mean and the median of the raw EVM distributions. Both parts of Fig. 14 have the same scale. The mean of the raw EVM distribution is equal to

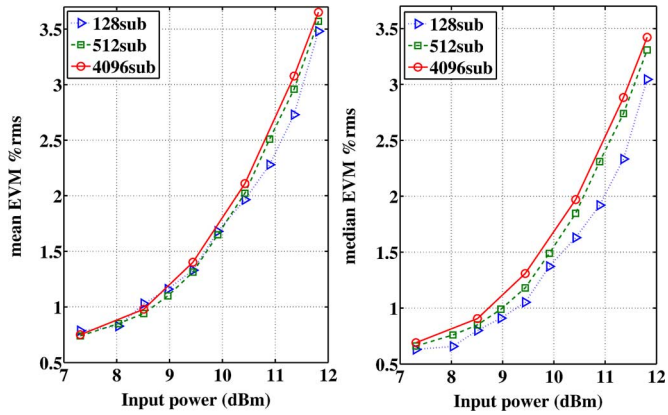

Fig. 14. Mean (*left*) and median (*right*) results of the raw EVM distributions versus input power.

the mean of the EVM per frame distribution (see Fig. 6), as expected from (12). The reduction in EVM when using the median compared to the mean is significant and becomes greater as the number of subcarriers is reduced, as expected from the trends in the skew result of Fig. 13. It can be seen that, for the median EVM results, the need for reduced back-off with lower numbers of subcarriers (lower PAPR) is more clearly observed.

VII. CONCLUSION

EVM measurement results for a directly modulated RoF link transporting a large number of OFDM frames with QPSK modulation have been presented. The mean EVM results (with the mean calculated over each OFDM frame) do not indicate that the amount of input power back-off required from P1 dB depends on the number of subcarriers (at least to the extent expected by the statistical PAPR for different numbers of subcarriers). The reason is found to be that with distortion, the raw EVM distributions are skewed, with the skew being higher for signals with lower numbers of subcarriers. The higher skew for these signals causes the mean to increase by a higher amount than signals with higher numbers of subcarriers, as the mean is more susceptible to outliers. However, when using the median of the raw EVM, differences in the EVM performance between signals with different numbers of subcarriers become more apparent. As a result, statistical PAPR can be related, in principle, with differences in the required input power back-off for these signals. The analysis method used in this paper can be applied to other nonlinear system (e.g., external modulation links) transporting OFDM signals, including other high bit-rate RoF systems and non-RoF systems, but would not apply in the case of single-carrier systems. Additionally, similar trends to those observed in the results presented in this paper are expected for such systems.

REFERENCES

[1] N. J. Gomes, M. Morant, A. Alphones, B. Cabon, J. E. Mitchell, C. Lethien, M. Csörnyei, A. Stöhr, and S. Iezekiel, "Radio-over-fiber transport for the support of wireless broadband services," *J. Opt. Netw.*, vol. 8, no. 2, pp. 156–178, Feb. 2009.

[2] M. Sauer, A. Kobyakov, and J. George, "Radio over fiber for picocellular network architectures," *J. Lightw. Technol.*, vol. 25, no. 11, pp. 3301–3320, Nov. 2007.

[3] Y. X. Guo, V. H. Pham, M. L. Yee, and L. C. Ong, "Improved radio-over-fiber transponder with multistage automatic gain control," *IEEE Trans. Microw. Theory Techn.*, vol. 57, no. 11, pp. 2816–2823, Nov. 2009.

[4] Z. Bouhamri, Y. Le Guennec, J. M. Duchamp, G. Maury, A. Schimpf, V. Dobremez, L. Bidaux, and B. Cabon, "Multistandard transmission over plastic optical fiber," *IEEE Trans. Microw. Theory Techn.*, vol. 58, no. 11, pp. 3109–3116, Nov. 2010.

[5] A. Nkansah, A. Das, N. J. Gomes, and P. Shen, "Multilevel modulated signal transmission over serial single-mode and multimode fiber links using vertical-cavity surface-emitting lasers for millimeter-wave wireless communications," *IEEE Trans. Microw. Theory Techn.*, vol. 55, no. 6, pp. 1219–1228, Jun. 2007.

[6] J. James, P. Shen, A. Nkansah, X. Liang, and N. J. Gomes, "Nonlinearity and noise effects in multi-level signal millimeter-wave over fiber transmission using single and dual wavelength modulation," *IEEE Trans. Microw. Theory Techn.*, vol. 58, no. 11, pp. 3189–3198, Nov. 2010.

[7] D. Wake, A. Nkansah, N. J. Gomes, G. de Valicourt, R. Brenot, M. Violas, Z. Liu, F. Ferreira, and S. Pato, "A comparison of radio over fiber link types for the support of wideband radio channels," *J. Lightw. Technol.*, vol. 28, no. 16, pp. 2416–2422, Aug. 2010.

[8] C. H. Cox, III, E. I. Ackerman, G. E. Betts, and J. L. Prince, "Limits on the performance of RF-over-fiber links and their impact on device design," *IEEE Trans. Microw. Theory Techn.*, vol. 54, no. 2, pp. 906–920, Feb. 2006.

[9] D. Dardari, V. Tralli, and A. Vaccori, "A theoretical characterization of nonlinear distortion effects in OFDM systems," *IEEE Trans. Commun.*, vol. 48, no. 10, pp. 1755–1764, Oct. 2000.

[10] J. Minkoff, "The role of AM-to-PM conversion in memoryless nonlinear systems," *IEEE Trans. Commun.*, vol. COM-33, no. 2, pp. 139–144, Feb. 1985.

[11] X. Li and L. J. Cimini, "Effects of clipping and filtering on the performance of OFDM," in *Proc. IEEE 47th Veh. Technol. Conf.*, Phoenix, AZ, USA, 1997, pp. 1634–1638.

[12] R. Gross and D. Veeneman, "Clipping distortion in DMT ADSL systems," *Electron. Lett.*, vol. 29, no. 24, pp. 2080–2081, Nov. 1993.

[13] R. O'Neill and L. N. Lopes, "Envelope variations and spectral splatter in clipped multicarrier signals," in *6th IEEE Int. Pers., Indoor, Mobile Radio Commun. Symp.*, 1995, pp. 71–75.

[14] M. R. D. Rodrigues, J. E. Mitchell, and I. Darwazeh, "On the error probability performance of non-linearly distorted OFDM signals," in *Proc. 57th IEEE Veh. Technol. Conf.*, 2003, pp. 1278–1282.

[15] P. Horvath and I. Frigyes, "Effects of the nonlinearity of a Mach–Zehnder modulator on OFDM radio-over-fiber transmission," *IEEE Commun. Lett.*, vol. 9, no. 10, pp. 921–923, Oct. 2005.

[16] T. Bercelii, M. Csornyei, B. Klein, and T. Banky, "Nonlinear effects in optical-wireless OFDM signal transmission," in *Int. Microw. Photon. Top. Meeting*, Awaji, Japan, 2002, pp. 225–228.

[17] B. Zhang, Y. Lu, J. Zhang, and B. Yang, "Nonlinear effect of OFDM in radio-over-fiber transmission," in *Int. Microw. Millimeter-Wave Technol. Conf.*, 2007, pp. 1–3.

[18] P. Assimakopoulos, L. Vieira, A. Nkansah, D. Wake, N. J. Gomes, and F. van Dijk, "Modelling of a DFB laser at low bias directly modulated with an OFDM signal for RoF applications," in *Proc. IEEE Int. Microw. Photon. Top. Meeting*, Valencia, Spain, 2009, pp. 1–4.

[19] D. Wake, A. Nkansah, and N. J. Gomes, "Radio over fiber link design for next generation wireless systems," *J. Lightw. Technol.*, vol. 28, no. 16, pp. 2456–2464, Aug. 2010.

[20] P. Banelli and S. Cacopardi, "Theoretical analysis and performance of OFDM signals in nonlinear AWGN channels," *IEEE Trans. Commun.*, vol. 48, no. 3, pp. 430–441, Mar. 2000.

[21] A. Papoulis, *Probability, Random Variables, and Stochastic Processes*, 3rd ed. New York, NY, USA: McGraw-Hill, 1991.

[22] L. Hanzo, M. Munster, B. J. Choi, and T. Keller, *OFDM and MC-CDMA for Broadband Multi-User Communications, WLANs and Broadcasting*. New York, NY, USA: Wiley, 2003.

[23] J. Tellado, *Multicarrier Modulation With Low PAR-Applications to DSL and Wireless*. Norwell, MA, USA: Kluwer, 2002.

[24] R. van Nee and A. de Wild, "Reducing the peak-to-average power ratio of OFDM," in *Proc. IEEE Veh. Technol. Conf.*, 1998, pp. 2072–2076.

[25] W. B. Davenport, Jr. and W. L. Root, *An Introduction to the Theory of Random Signals and Noise*. New York, NY, USA: IEEE Press, 1987.

[26] H. Ochiai and H. Imai, "Performance analysis of deliberately clipped OFDM signals," *IEEE Trans. Commun.*, vol. 50, no. 1, pp. 89–101, Jan. 2002.

[27] J. Andrews, A. Ghosh, and R. Muhamed, *Fundamentals of WiMAX*. Englewood Cliffs, NJ, USA: Prentice-Hall, 2007.

[28] M. D. McKinley, K. A. Remley, M. Myslinski, J. S. Kenney, D. Schreurs, and B. Nauwelaers, "EVM calculation for broadband modulated signals," in *64th ARFTG Conf. Dig.*, 2004, pp. 45–52.

[29] J. D. Jobson, *Applied Multivariate Data Analysis: Regression and Experimental Design*. Berlin, Germany: Springer, 1991.

[30] E. Limpert, W. A. Stahel, and M. Abbt, "Log-normal distributions across the sciences: Keys and clues," *BioScience*, vol. 51, no. 5, pp. 341–352, May 2001. [Online]. Available: http://stat.ethz.ch/~stahel/lognormal/bioscience.pdf

Philippos Assimakopoulos received the B.Eng. degree in electronic engineering from the University of Bath, Bath, U.K., in 2003, and the M.Sc. degree in broadband and mobile communication networks and Ph.D. degree in electronic engineering from the University of Kent, Canterbury, U.K., in 2007 and 2012, respectively.

He is currently with the Broadband and Wireless Communications Group, University of Kent. His research interests include low-cost microwave RoF networks for indoor and outdoor applications.

Anthony Nkansah received the B.Eng. degree (with honors) in electronic engineering, M.Sc. degree in broadband and mobile communication networks, and Ph.D. degree in electronic engineering from the University of Kent, Canterbury, U.K., in 2000, 2001, and 2007, respectively.

He is currently with the Broadband and Wireless Communications Group, University of Kent. His research interests include low-cost microwave and millimeter-wave RoF networks and their deployment within premises.

Nathan J. Gomes (M'92–SM'06) received the B.Sc. degree from the University of Sussex, Sussex, U.K., in 1984, and the Ph.D. degree from University College London, London, U.K., in 1988, both in electronic engineering.

From 1988 to 1989, he held a Royal Society European Exchange Fellowship with ENST, Paris, France. Since late 1989, he has been with the University of Kent, Canterbury, U.K., where he is currently a Reader in broadband communications. His current research interests include RoF systems and networks, the photonic generation and transport of millimeter-wave signals, and photo-receivers for such applications.

David Wake (M'03) received the B.Sc. degree in applied physics from the University of Wales, Cardiff, U.K., in 1979, and the Ph.D. degree from the University of Surrey, Surrey, U.K., in 1987.

He is currently a Senior Research Fellow with the University of Kent, Canterbury, U.K. From 2003 to 2005, he was the Director of Research and Development and Chief Scientist with Microwave Photonics Inc., Los Angeles, CA, USA, a startup company that was formed to develop a product set for the mobile communications industry based on novel RoF technology. In 2002, he co-founded Zinwave Ltd., a startup company aimed at exploiting innovative RoF technology for the mobile communications industry. He has been involved in RoF research for over 20 years, initially with BT Laboratories, where he was the Program Manager for the microwave photonics research domain, and then with University College London, as a Senior Research Fellow.